



HAL
open science

Synthesis of magnetite, ceria and magnetite-ceria materials by calcination of nanostructured precursor-minerals

German Montes-Hernandez

► **To cite this version:**

German Montes-Hernandez. Synthesis of magnetite, ceria and magnetite-ceria materials by calcination of nanostructured precursor-minerals. *Materials Letters*, 2020, 276, pp.128246. 10.1016/j.matlet.2020.128246 . hal-02896883

HAL Id: hal-02896883

<https://hal.science/hal-02896883>

Submitted on 5 Nov 2020

HAL is a multi-disciplinary open access archive for the deposit and dissemination of scientific research documents, whether they are published or not. The documents may come from teaching and research institutions in France or abroad, or from public or private research centers.

L'archive ouverte pluridisciplinaire **HAL**, est destinée au dépôt et à la diffusion de documents scientifiques de niveau recherche, publiés ou non, émanant des établissements d'enseignement et de recherche français ou étrangers, des laboratoires publics ou privés.

25 **Abstract**

26 The present short communication reports an original experimental calcination method to
27 synthesize magnetic materials with high thermal stability such as magnetite (Fe_3O_4) with typical
28 spinel and atypical crystal shape, sub-micrometric rounded crystals of ceria (CeO_2) and magnetite-
29 ceria composites with varied shape and size of crystals; these latter depending on the nature of
30 mineral precursors (goethite, siderite or ferrihydrite). Herein, it was demonstrated that cooperative
31 redox reactions and simple vacuum can be used to synthesize magnetic composite materials by
32 calcination of nanostructured mineral precursors. In this way, bastnäsite mineral (CeCO_3F) is a
33 powerful reducing agent to synthesize magnetite from reductive dehydration of ferric
34 oxyhydroxides.

35

36

37 **Keywords:** Magnetic materials; Composites, Crystallization; Electron microscopy.

38

39 1. Introduction

40 Synthetic ceria (CeO_2) and magnetite (Fe_3O_4) are crucial oxides in many industrial and/or medical
41 applications related to their extraordinary chemical properties (acid-base and oxidation-reduction
42 behavior), thermal stability and oxygen mobility [1-6]. They have found their applications in
43 catalysis (photo-), luminescent materials, fuel cell, free radical scavenger, gas sensor, cosmetic
44 material, optical additives, polishing materials, water splitting, ceramic pigments, biomedicine,
45 magnetic storage media, etc. [1-6]. In general, magnetite or ceria are independently used; however,
46 recently their association as magnetite-ceria composites have been also explored in catalytic
47 reactions, for example, in the degradation of organic molecules [7], in Fenton reactions [8], in
48 multicomponent redox reactions [9] and in the dephosphorylation of phosphopeptides [10]. In this
49 way, the improving of existing methods and/or developing innovative routes to obtain well-
50 controlled crystal shapes and sizes remain important challenges in materials science. The present
51 short communication reports an original calcination method to synthesize magnetite, ceria and
52 magnetite-ceria composites with high thermal stability and probably with relevant catalytic
53 properties by using dynamic vacuum ($\approx 5 \times 10^{-6}$ mbar) and bastnäsite (CeCO_3F) nanostructured
54 mineral as reducing agents. In fact, four nanostructured minerals goethite ($\text{FeO}(\text{OH})$), siderite
55 (FeCO_3), ferrihydrite 6-lines and bastnäsite (CeCO_3F) were synthesized at low T ($< 95^\circ\text{C}$), methods
56 already published by my group [11-14]. Then the obtained nanostructured minerals are used as
57 powdered precursors in order to synthesize magnetite from reductive dehydration of goethite or
58 from oxidative decarbonation of siderite, ceria from oxidative decarbonation of bastnäsite and
59 magnetite-ceria composites from cooperative and/or competitive redox reactions. Mineral
60 composition and crystal shape and size were mainly determined by XRD and FESEM.

61 **2. Materials and Methods**

62 *2.1. Synthesis of mineral precursors and nano-magnetite reference*

63 Goethite, siderite, ferrihydrite and bastnäsite minerals were synthesized by using already published
64 methods [11-14]. In supplementary information, only the overall reaction of synthesis of precursor
65 and magnetite reference, including a basic characterization by XRD and FESEM are provided
66 (Figure SI-1).

67 *2.2. Synthesis of magnetite, ceria and magnetite-ceria composites*

68 *Magnetite from oxidative decarbonation of siderite*

69 2g of dry siderite placed in an alumina ceramic crucible were calcinated at 500°C under secondary
70 vacuum ($\approx 5 \times 10^{-6}$ mbar) for 5h by using a quartz tubular reactor. A heating rate of 30°C/min was
71 performed in all experiments. At the end of experiment, the calcinated product were cooled under
72 dynamic vacuum at room temperature ($\sim 19^\circ\text{C}$).

73 *Magnetite from reductive dehydration of goethite*

74 1g of dry goethite and 1g of dry bastnäsite placed independently in an alumina ceramic crucible
75 (e.i. without solid-solid contact) were calcinated at the same above conditions. In this case, the
76 bastnäsite transformation into ceria (CeO_2) improves the reducing conditions in the reactor
77 allowing complete goethite transformation into magnetite.

78 *Ceria from oxidative decarbonation of bastnäsite*

79 2g of dry bastnäsite placed in an alumina ceramic crucible were calcinated at the same above

80 conditions.

81 *Synthesis Fe₃O₄- CeO₂ composites*

82 Three different binary mineral-precursor mixtures (ferrihydrite-bastnäsite, goethite-bastnäsite and
83 siderite-bastnäsite) were manually prepared by using equivalent weighs in an agate mortar and
84 mixed by a pestle. Then, 2g of each mineral mixture were placed in an alumina ceramic crucible
85 and calcinated at the same above conditions.

86 All calcinated solid products were manually recovered and stored in plastic flasks for subsequent
87 characterization by XRD and FESEM (see supplementary information).

88

89 **3. Results and Discussion**

90 All main results are summarized in Figures 1 to 3 concerning particularly FESEM images and DRX
91 patterns of calcinated products. Based on this conventional solid characterization for precursors
92 (Figure SI-1) and calcinated products, an overall redox reaction for each investigated scenario is
93 suggested as follows:

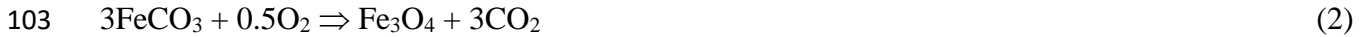
94 Magnetite formation from goethite



96 The formation of magnetite is improved when bastnäsite mineral is used as supplementary reducing
97 agent in the reactor (see Figure SI-2). In such case, the Ce(III) oxidation to Ce(IV) initially
98 contained in cerium carbonate creates a most reducing atmosphere into the reactor during
99 calcination process. FESEM images have revealed two crystals shapes of magnetite, typical spinel
100 shape and acicular crystals; letter shape was probably inherited from original goethite shape (Figure

101 1).

102 Magnetite formation from siderite decarbonation



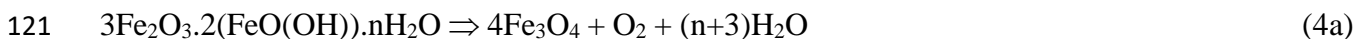
104 The constrained dynamic vacuum was enough to favor the magnetite formation rather than
105 hematite (Fe_2O_3). Assuming that water is also present in the system (residual water in vacuum
106 atmosphere), the following oxidative reaction ($3\text{FeCO}_3 + \text{H}_2\text{O} \Rightarrow \text{Fe}_3\text{O}_4 + 3\text{CO}_2 + \text{H}_2$) could also
107 contribute to magnetite formation. Surprisingly, synthesized magnetite have conserved the initial
108 shape of siderite spherical aggregates as revealed by FESEM, however, the magnetite micrometric
109 ($<3\mu\text{m}$) spherical agglomerates constituted by magnetite nanoparticles are now observed (Figure
110 1).

111 Ceria formation from bastnäsite decarbonation



113 This reaction can be auto-enhanced by in situ produced fluorine than can react with residual water in
114 the system to form additional oxidants (e.g. $\text{F}_2 + \text{H}_2\text{O} \Rightarrow 0.5\text{O}_2 + 2\text{HF}$). However, the XRD has
115 also revealed cerium oxide fluoride (CeOF) that is generally a transient phase during ceria
116 formation from oxidative decarbonation of bastnäsite ($\text{CeCO}_3\text{F} \Rightarrow \text{CeOF} + \text{CO}_2$) with a short
117 lifetime under air atmosphere as already demonstrated [12]. Finally, FESEM images have revealed
118 rounded ceria nanoparticles with high agglomeration degree with respect to ceria formed under air
119 atmosphere (see Figure 2).

120 Magnetite-Ceria composite from ferrihydrite-bastnäsite mixture



123 A complete transformation of ferrihydrite into magnetite was particularly possible by means of
124 cerium oxidation contained in bastnaesite. This means that a cooperative double-redox reaction
125 exists: $\text{Fe}^{3+}/\text{Fe}^{2+}$ and O^{2-}/O_2 for magnetite formation and $\text{Ce}^{3+}/\text{Ce}^{4+}$, O_2/O^{2-} and F^-/F_2 for ceria
126 formation. In terms of mineral composition, the XRD has revealed magnetite and ceria as major
127 phases and a minor proportion of cerium oxide fluoride (CeOF) and sodium fluoride (NaF) were
128 also detected in final products, indicating an incomplete oxidation of cerium initially contained in
129 bastnäsite mesocrystals (see XRD patterns in Figure 3). FESEM images have revealed
130 homogeneous mixture of micrometer magnetite crystal ($<2\mu\text{m}$) with spinel shape and sub-
131 micrometric ceria crystals with rounded shape. Ceria particles adhered onto magnetite crystals or
132 forming aggregates.

133 Magnetite-Ceria composite from goethite-bastnäsite mixture



136 This cooperative double redox reaction is identical to ferrihydrite-bastnäsite system, however,
137 different crystal shape and size and different water content exist between goethite and ferrihydrite
138 (see Figure SI-1). As expected, magnetite-ceria composite was synthesized as revealed from XRD
139 patterns. In this case, sub-micrometric magnetite crystals with spinel shape are homogeneously
140 mixed with nanometric ceria rounded-crystals having high agglomeration and/or aggregation
141 degree as observed in the FESEM image (Figure 3).

142 Magnetite-Ceria composite from siderite-bastnäsite mixture



145 Contrary to two above cooperative redox systems, here, an oxidative-decarbonation competition
146 exists as illustrated in reactions 6a and 6b. Despite this competition, the magnetite-ceria composite
147 was successfully synthesized as revealed by XRD (Figure 3). However, a more reducing
148 environment in the reactor was created because a higher proportion of cerium oxide fluoride
149 (CeOF) and also iron oxide (FeO) were detected; both mineral phases implying only decarbonation
150 process without oxidation, possible only in high reducing systems. FESEM images have revealed
151 sub-micrometric magnetite and ceria crystals with rounded shape and with high agglomeration
152 degree (see Figure 3 and Figure SI-3).

153

154 **4. Conclusion**

155 Magnetite with typical spinel and atypical crystal shape, sub-micrometric rounded crystals of ceria
156 and magnetite-ceria composites with varied shape and size of crystals were synthesized by
157 calcination under dynamic secondary vacuum and using bastnäsite as complementary solid
158 reducing agent.

159

160

161

162

163

164

165 **Acknowledgements**

166 The authors are grateful to CNRS and UGA for providing funding support. IPAG is grateful for
167 allowing the access to calcination experiments. We thank Nathaniel Findling, Olivier Brissaud,
168 Pierre Beck and Eric Quirico for their technical assistance.

169

170

171

172

173

174

175

176

177

178

179

180

181

182

183

184

185

186

187 **References**

188 [1] A. Bumajdad, J. Eastoe, A. Mathew, Cerium oxide nanoparticles prepared in self-assembled
189 systems, *Adv. Colloid Interface Sci.* 147-148 (2009) 56-66.

190 [2] E. Leino, P. Maki-Arvela, V. Eta, N. Kumar, F. Demoisson, A. Samikannu, A. R. Leino, A.
191 Shchukarev, D. Y. Murzin, J. P. Mikkola, The influence of various synthesis methods on the
192 catalytic activity of cerium oxide in one-pot synthesis of diethyl carbonate starting from CO₂,
193 ethanol and butylene oxide, *Catalysis Today* 210 (2013) 47-54.

194 [3] N. Gokon, S. Sagawa, T. Kodoma, Comparative study of activity of cerium oxide at thermal
195 reduction temperatures of 1300–1550 °C for solar thermochemical two-step water-splitting cycle,
196 *Int. J. Hydrogen Energy* 38 (2013) 14402-14414.

197 [4] J. Mosayebi, M. Kiyasatfar, S. Laurent, Synthesis, functionalization, and design of magnetic
198 nanoparticles for theranostic applications, *Adv. Healthcare Mater.* (2017) 1700306

199 [5] M. Usman, J. M. Byrne, A. Chaudhary, S. Orsetti, K. Hanna, C. Ruby, A. Kappler, S. B.
200 Haderlein, Magnetite and green Rust: synthesis, properties, and environmental applications of
201 mixed-valent iron minerals, *Chem. Rev.* 118 (2018) 3251–3304.

202 [6] J. Jolivet, C. Chanéac, E. Tronc, Iron oxide chemistry. From molecular clusters to extended
203 solid networks, *Chem. Commun.* (2004) 481–487.

204 [7] G. Gan, P. Zhao, X. Zhang, J. Liu, J. Liu, C. Zhang, X. Hou, Degradation of Pantoprazole in
205 aqueous solution using magnetic nanoscaled Fe₃O₄/CeO₂ composite: Effect of system parameters
206 and degradation pathway, *J. Alloy. Compd.* 725 (2017) 472-483.

- 207 [8] L. Xu, J. Wang, Magnetic Nanoscaled Fe₃O₄/CeO₂ Composite as an Efficient Fenton-Like
208 Heterogeneous Catalyst for Degradation of 4-Chlorophenol, *Environ. Sci. Technol.* 46, (2012)
209 10145–10153.
- 210 [9] M. B. Gawande, V. D. B. Bonifácio, R. S. Varma, I. D. Nogueira, N. Bundaleski, C. A. A.
211 Ghumman, O. M. N. D. Teodoro, P. S. Branco, Magnetically recyclable magnetite–ceria (Nanocat-
212 Fe-Ce) nanocatalyst – applications in multicomponent reactions under benign conditions, *Green*
213 *Chem.* 15, (2013) 1226-1231.
- 214 [10] Q. Min, S. Li, X. Chen, E. S. Abdel-Halim, L.-P. Jiang, J.-J. Zhu, Magnetite/ceria-codecorated
215 titanoniobate nanosheet: A 2D catalytic nanoprobe for efficient enrichment and programmed
216 dephosphorylation of phosphopeptides, *ACS Appl. Mater. Interfaces* 7 (2015) 9563–9572.
- 217 [11] S. Hajji, G. Montes-Hernandez, G. Sarret, A. Tordo, G. Morin, G. Ona-Nguema, S. Bureau,
218 T. Turki, M. Nzoughi, Arsenite and chromate sequestration onto ferrihydrite, siderite and goethite
219 nanostructured minerals: Isotherms from flow-through reactor experiments and XAS
220 measurements, *J. Hazard. Mater.* 362 (2019) 358-367.
- 221 [12] G. Montes-Hernandez, R. Chiriac, N. Findling, F. Toche, F. Renard, Synthesis of Ceria (CeO₂
222 and CeO_{2-x}) Nanoparticles via Decarbonation and Ce(III) Oxydation of Synthetic Bastnäsite
223 (CeCO₃F_x), *Mater. Chem. Phys.* 172 (2016) 202-210.
- 224 [13] G. Montes-Hernandez, P. Beck, F. Renard, E. Quirico, B. Lanson, R. Chiriac, N. Findling,
225 Fast precipitation of acicular goethite from ferric hydroxide gel under moderate temperature (30
226 and 70 C degrees), *Cryst. Growth Des.* 11 (2011) 2264-2272.

227 [14] G. Montes-Hernandez, F. Renard, Time-resolved in situ Raman spectroscopy of the nucleation
228 and growth of siderite, magnesite and calcite and their precursors, *Cryst. Growth Des.* 16 (2016)
229 7218-7230.

230

231

232

233

234

235

236

237

238

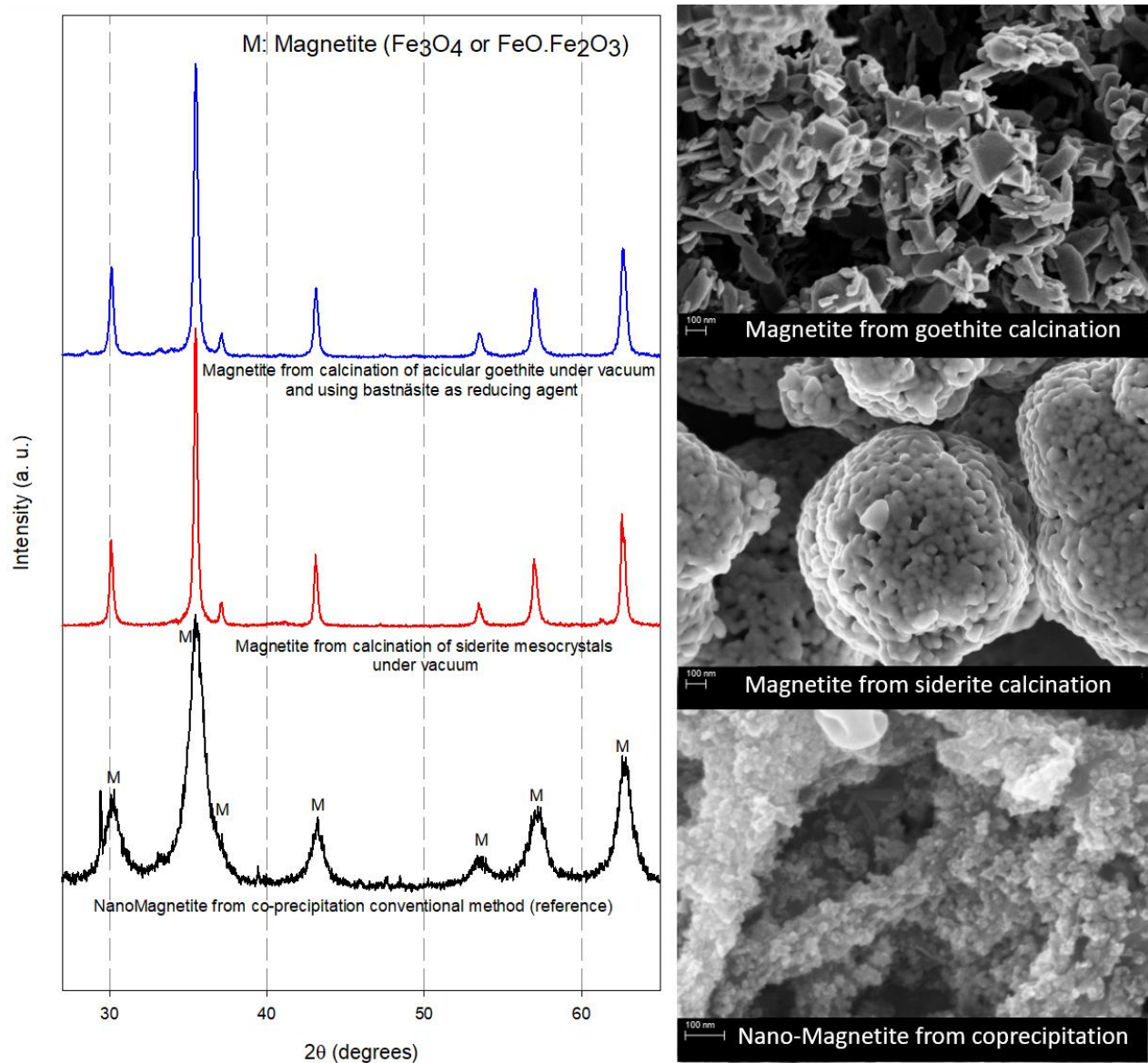
239

240

241

242

243



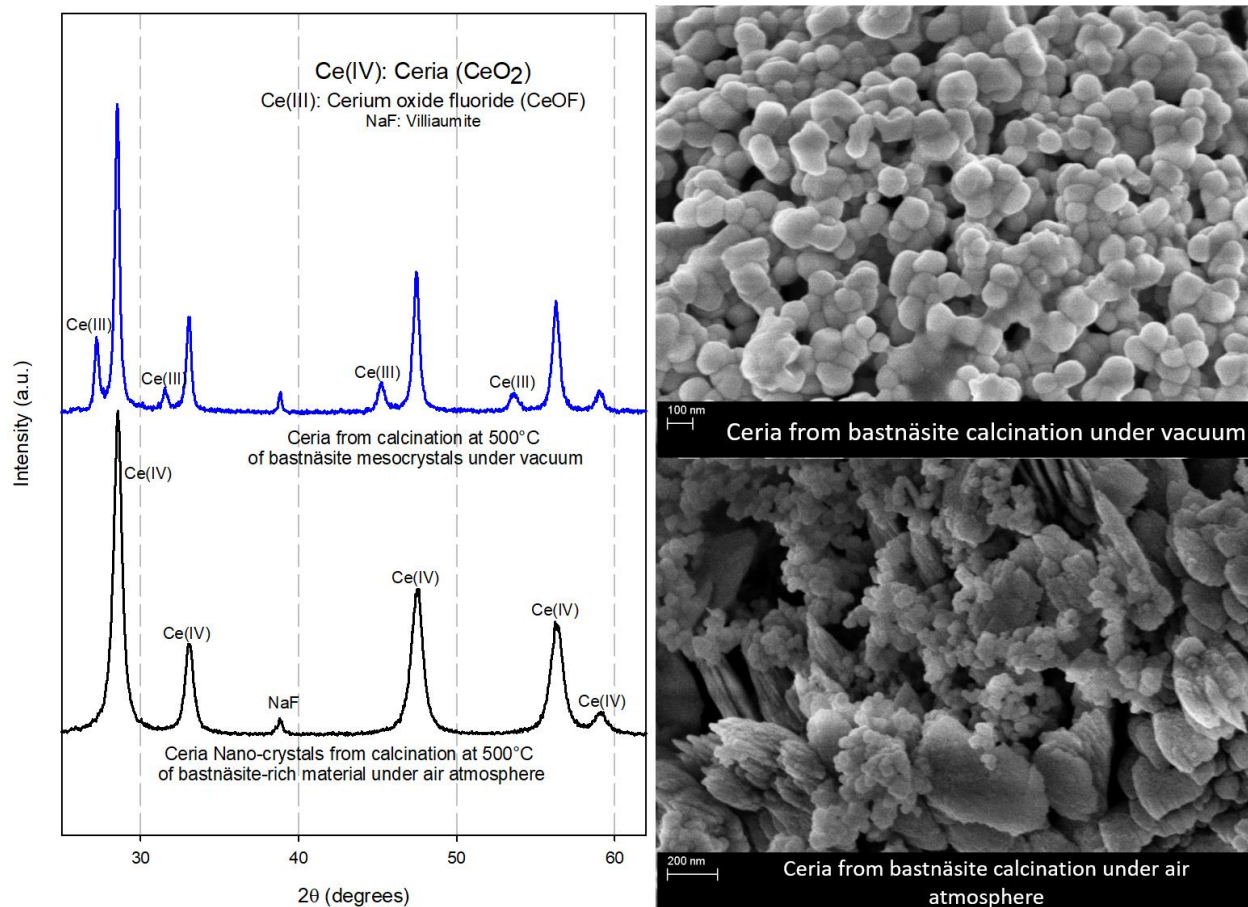
244

245

246

247 Figure 1. XRD patterns for three magnetite synthesized for three different reaction pathways and

248 FESEM images showing shape and size of magnetite crystals.



249

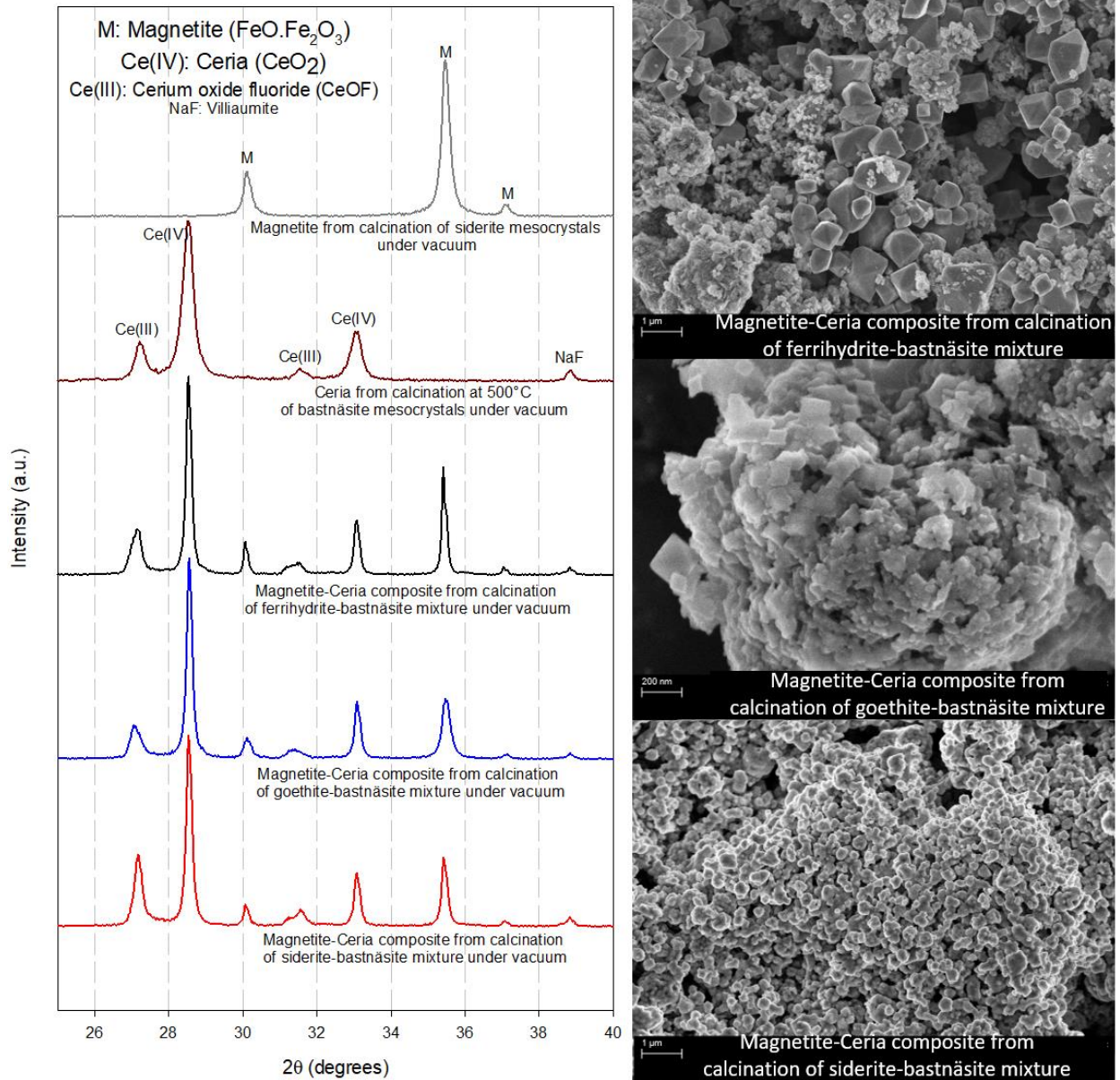
250

251 Figure 2. XRD patterns for two ceria synthesized under air atmosphere (reference) and under
 252 dynamic vacuum and FESEM images showing shape and size of ceria crystals.

253

254

255



256

257 Figure 3. XRD patterns for three magnetite-ceria composite materials synthesized by calcination

258 of three different mineral-precursor mixtures and FESEM images showing shape and size of

259 magnetite crystals.

260